

Quantum nature of a strongly coupled single quantum dot–cavity system

K. Hennessy^{1,2*}, A. Badolato^{1*}, M. Winger^{1*}, D. Gerace¹, M. Atatüre¹, S. Gulde¹, S. Fält¹, E. L. Hu² & A. Imamoglu¹

Cavity quantum electrodynamics (QED) studies the interaction between a quantum emitter and a single radiation-field mode. When an atom is strongly coupled to a cavity mode^{1,2}, it is possible to realize important quantum information processing tasks, such as controlled coherent coupling and entanglement of distinguishable quantum systems. Realizing these tasks in the solid state is clearly desirable, and coupling semiconductor self-assembled quantum dots to monolithic optical cavities is a promising route to this end. However, validating the efficacy of quantum dots in quantum information applications requires confirmation of the quantum nature of the quantum-dot–cavity system in the strong-coupling regime. Here we find such confirmation by observing quantum correlations in photoluminescence from a photonic crystal nanocavity^{3–5} interacting with one, and only one, quantum dot located precisely at the cavity electric field maximum. When off-resonance, photon emission from the cavity mode and quantum-dot excitons is anticorrelated at the level of single quanta, proving that the mode is driven solely by the quantum dot despite an energy mismatch between cavity and excitons. When tuned to resonance, the exciton and cavity enter the strong-coupling regime of cavity QED and the quantum-dot exciton lifetime reduces by a factor of 145. The generated photon stream becomes antibunched, proving that the strongly coupled exciton/photon system is in the quantum regime. Our observations unequivocally show that quantum information tasks are achievable in solid-state cavity QED.

Pursuit of solid-state cavity QED is motivated by the possibility of fixing the emitter location with respect to the cavity mode electric field maximum and of enhancing the emitter–cavity coupling by fabricating cavities with ultrasmall volumes. Substantial progress has been made to this end, culminating in the demonstration of strong coupling of a Cooper pair box to a superconducting transmission line microwave resonator⁶ and of a semiconductor self-assembled quantum dot (QD) to a nanoscale optical cavity mode^{7–9}. However, further progress in QD cavity QED has been partially hindered by the conventional practice of incorporating many QDs at random locations in the cavity, leading to indirect/off-resonant coupling to other QDs overlapping the mode. Recent experiments showing intense cavity emission, and even lasing, when the mode is non-resonant with the QDs^{4,7–10} suggest that observation of quantum effects would require a nanocavity containing a single QD.

Here we demonstrate a new technique to locate the absolute position of buried QDs by atomic force microscopy (AFM) metrology. As the top half of the photonic crystal slab is grown on the QD layer (see Methods), the presence of the QDs gives rise to small but distinctive 1–2 nm hills on the surface that can be detected by AFM. In ways similar to those used to position nanocavities relative to stacks of QDs¹⁰, we were able to position with 30 nm accuracy a nanocavity

relative to one, and only one, QD, aligning it to the electric-field maximum of the cavity mode as shown in Fig. 1a, b. This positioning technique allows us to study the coupled system with unprecedented clarity. Furthermore, in comparison to devices containing multiple QDs, we achieve significantly higher quality factors (*Q*s), ranging from 12,000 to 30,000 in ~20 deterministically coupled devices. In typical devices, QDs are located at ~90% of the electric-field maximum.

Our approach allows for pre-selection of QDs with desirable spectral properties. In the remainder of this Letter, we follow one such QD that was selected on the basis of a small QD–mode spectral detuning despite having less-than-average QD–mode alignment. The measured photoluminescence spectrum (see Methods) of this QD (Fig. 1c) consisted of a few narrow, isolated excitonic transitions that were promising for nanocavity coupling. We then fabricated^{10,11} the

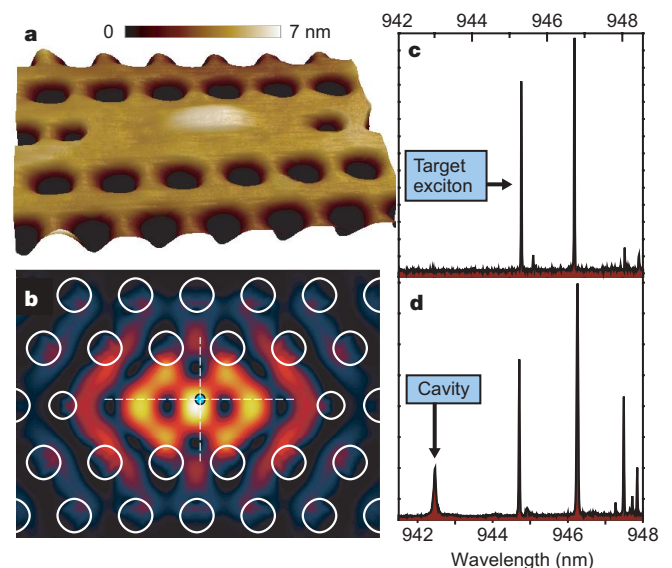


Figure 1 | Positioning a photonic crystal cavity mode relative to a single buried QD. **a**, AFM topography of a photonic crystal nanocavity aligned to a hill of material on the surface arising from a QD buried 63 nm below. The height scale is depicted by the colour bar. **b**, Electric field intensity of the photonic crystal cavity mode showing that the location of the buried QD, indicated by the teal dot, overlaps the field maximum. The field intensity ranges from zero (black) to a maximum (white), going through blue, red and yellow. **c**, Photoluminescence spectrum before cavity fabrication of a single QD, which was selected for cavity coupling on the basis of clear emission from a few discrete excitonic transitions. **d**, Photoluminescence spectrum from the same QD after cavity fabrication, showing emission from the cavity at 942.5 nm.

¹Institute of Quantum Electronics, ETH Zürich, HPT G10, 8093 Zurich, Switzerland. ²California NanoSystems Institute, University of California, Santa Barbara, California 93106, USA. *These authors contributed equally to this work.

photonic crystal with the lattice parameter a and hole radius r/a selected to lithographically tune the nanocavity mode to this precise spectral location. As shown in Fig. 1d, the cavity mode is spectrally positioned a few nanometres shorter in wavelength than the exciton transitions, allowing us to tune the cavity by a thin-film condensation technique¹² and study the exciton–cavity interaction as a function of the detuning between mode and exciton, $\Delta_\lambda = \lambda_x - \lambda_m$ ($\Delta_\omega = \omega_m - \omega_x$), where λ_x (ω_x) and λ_m (ω_m) denote the resonant exciton and cavity-mode wavelength (angular frequency), respectively.

An important feature of the spectrum in Fig. 1d is that emission from the cavity mode is observed where there was clearly no QD emission before cavity fabrication. Cavity emission for arbitrary detunings challenges the notion that QDs may be fully described as artificial atoms with discrete energy levels. To explain this effect, recent reports speculate that the mode is fed by either a background continuum or a multi-QD effective continuum⁷. We rule out the former by noting that no mode emission occurs for control cavities containing an InAs wetting layer but positively no QDs, and we dismiss the latter by observing that even a single QD sustains efficient mode emission for all detunings observed in our devices ($-19 \text{ nm} < \Delta_\lambda < 4.1 \text{ nm}$). We further investigate the nature of the off-resonant coupling by measuring the quantum correlations between photons emitted from the exciton transitions and the spectrally detuned ($\Delta_\lambda = 4.1 \text{ nm}$) cavity. This measurement corresponds to the second-order, normally ordered, cross-correlation function¹³ $g_{x,m}^{(2)}(\tau) = \langle : I_x(t+\tau)I_m(t) : \rangle / \langle I_x(t) \rangle \langle I_m(t) \rangle$, where $I_{x(m)}(t)$ and $I_{x(m)}(t+\tau)$ refer to the intensity of the exciton (cavity-mode) photon stream at time t and a delayed time $t+\tau$, respectively. Arrival of a cavity (exciton) photon triggers a timer that stops upon detection of an exciton (cavity) photon for a positive (negative) difference in arrival time (see Fig. 2a and Methods). We accumulate a histogram of the detection events (Fig. 2b). For zero time difference, we observe strong antibunching, a deviation from the uncorrelated case of $g^{(2)}(0) = 1$ that directly proves the two emission events stem from the same single quantum emitter and are anticorrelated at the level of single quanta. Remarkably, the time constant for negative time delay

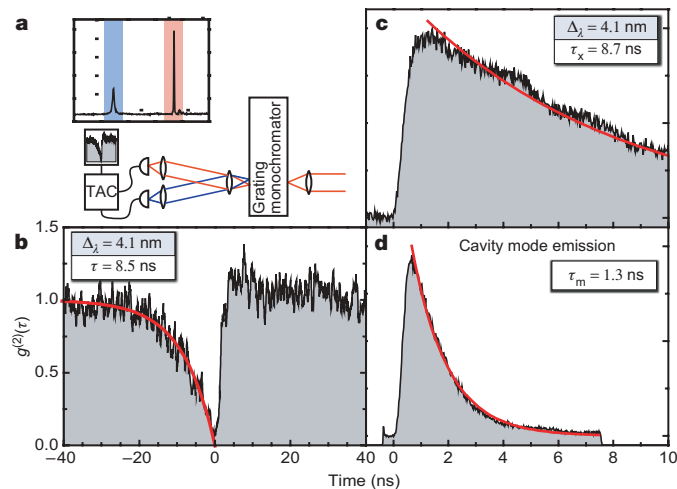


Figure 2 | Cross-correlation histogram and time-resolved photoluminescence from the QD–cavity system with $\Delta_\lambda = 4.1 \text{ nm}$. **a**, Diagram of the optical system used in cross-correlation measurements. The mode and exciton wavelengths are filtered as indicated by the blue and red shading, separated by a grating monochromator and imaged on separate single-photon detectors. **b**, Cross-correlation histogram of the mode and exciton emission (black) with exponential fits (red). The two emission events are anticorrelated at the single-photon level, giving rise to an antibunching in $g^{(2)}(\tau)$. **c**, The exciton lifetime $\tau_x = 8.7 \text{ ns}$ is comparable to the time constant observed in the cross-correlation histogram for negative time differences. **d**, The lifetime of the mode emission $\tau_m = 1.3 \text{ ns}$ is comparable to the time constant observed in the cross-correlation histogram for positive time differences.

2

(8.5 ns) corresponds to the lifetime of the exciton, $\tau_x = 8.7 \text{ ns}$ (Fig. 2c), while the time constant for positive time delay compares to the lifetime of the mode emission, $\tau_m = 1.3 \text{ ns}$ (Fig. 2d). (This is surprising because we would expect the lifetime of the states producing the stop pulse to dictate the respective time constant.) Off-resonant cavity–exciton anticorrelation demonstrates the existence of a new, unidentified mechanism for channelling QD excitations into a non-resonant cavity mode, indicating a clear deviation from a simple artificial atom model of the QD.

Having studied the exciton–mode coupling for large detuning, we then tuned the mode into resonance with the exciton to study resonant interaction. Clear evidence of the strong-coupling regime of cavity QED is obtained from spectra recorded as a function of Δ_λ . A subset of these spectra is plotted in Fig. 3b, from which we note the following features: for $\Delta_\lambda > 0.05 \text{ nm}$, the short-wavelength spectral feature remains cavity-like with a linewidth of $\Delta\lambda_- \approx \Delta\lambda_m = 0.071 \text{ nm}$ and the long-wavelength peak retains its excitonic nature with $\Delta\lambda_+ \approx \Delta\lambda_x = 0.025 \text{ nm}$. Here, $\Delta\lambda_m$ ($\Delta\lambda_x$) denotes the bare cavity-mode (exciton) linewidth. For further decrease in Δ_λ , the short-wavelength feature broadens and then separates into two distinct peaks. As tuning proceeds, the middle peak preserves exactly the wavelength, linewidth and polarization of the cavity mode while the long- and short-wavelength peaks repel each other and assume equal linewidths of $\Delta\lambda_\pm = 0.042 \text{ nm} \approx (\Delta\lambda_m + \Delta\lambda_x)/2$. Our observation of a spectral triplet in the strong-coupling regime is unique among recent reports of solid-state vacuum Rabi splitting^{7–9}. The two outer peaks at $\Delta_\lambda = 0$ anticross, as shown in Fig. 3a, and are identified as the polariton states of the strongly coupled exciton–photon system. Their resonant frequencies Ω_\pm and linewidths Γ_\pm are:

$$\Omega_\pm + i\Gamma_\pm/2 = \frac{\omega_m + \omega_x}{2} - i\frac{\gamma_x + \gamma_m}{4} \pm \sqrt{g^2 + \frac{1}{4} \left(\Delta_\omega - i\frac{\gamma_x - \gamma_m}{2} \right)^2} \quad (1)$$

where g is the exciton–mode coupling frequency estimated from the minimum observed polariton splitting and the full-width at half-maximum (FWHM) of the mode $\gamma_m = 24.1 \text{ GHz} = 100 \mu\text{eV}$ ($Q \approx 13,300$) and exciton $\gamma_x = 8.5 \text{ GHz} = 35 \mu\text{eV}$. The calculated peak positions are plotted as the continuous lines in Fig. 3a, and show very good agreement with the measured ones. From this Rabi splitting trend, we find $g = 18.4 \text{ GHz} = 76 \mu\text{eV}$ and note that g is reduced to $\sim 70\%$ of its maximum possible value owing to the slight spatial

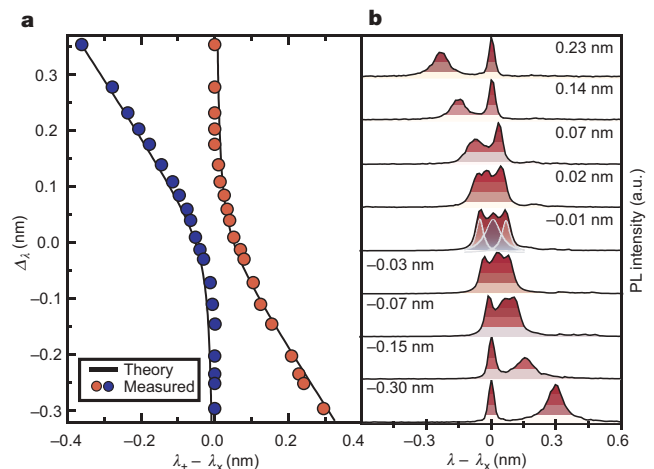


Figure 3 | Characteristics of the strong-coupling regime in the spectral domain. **a**, Wavelength of the polaritons for various detunings, Δ_λ . Calculated spectral peak positions describing the strongly coupled system are plotted as solid lines, with measured peak positions extracted from photoluminescence plotted in red and blue dots. **b**, Spectra of the two anticrossing polariton states near zero detuning. An additional peak is identified as the pure photonic state of the cavity. Values of Δ_λ are shown for each spectrum. PL, photoluminescence; a.u., arbitrary units.

mismatch between the QD and the electric field maximum of the cavity mode. Coupling constants for other instances of strong coupling with different excitons are as high as 120 μeV in our samples.

The predicted strong-coupling spectrum accounts for two of the three peaks that we observe experimentally—we attribute the additional peak to the pure photonic state of the cavity. A similar three-peak lineshape has been observed for Ba atoms strongly coupled to a high-finesse cavity¹⁴, and is attributed to fluctuations in the number of atoms present in the cavity over time. Our data can be regarded as the solid-state analogue of this scenario, in which fluctuations in emitter energy, rather than emitter number, occur over time. As the occupation of charging centres in the vicinity of the QD fluctuates, the exciton energy is renormalized via the Coulomb interaction and the detuning becomes large, $|\Delta_\omega| \gg g$. For such large detunings, the short-wavelength polariton reverts to the pure photonic state of the cavity. It is plausible that the QD exciton emission in this case leads to one of the longer-wavelength photoluminescence lines depicted in Fig. 1d. In our experiments, we integrate the photoluminescence for ~ 1 s, thereby collecting a time-average of the two regimes that results in the observed spectral triplet.

The clear signatures of strong coupling in Fig. 3 are confirmed by measuring τ_x as the mode is tuned into resonance with the exciton. Modification of τ_x is predicted to be particularly strong in a photonic crystal environment owing to the depleted density of optical states for energies in the photonic bandgap¹⁵. This is confirmed by our measurement at large detuning ($\Delta_\lambda = 4.1$ nm) of $\tau_x = 8.7$ ns, which is long in comparison to the lifetime in bulk material, $\tau_0 \approx 1$ ns. On the other hand, as the cavity mode spectrally approaches the exciton, τ_x should decrease owing to an effect that can be considered the counterpart of the Purcell effect^{16,17} for a detuned, strongly coupled system. As the cavity is tuned into resonance, τ_x decreases rapidly to $\tau_x \approx 1.6$ ns at $\Delta_\lambda = 1.26$ nm and further diminishes to a carrier-capture limited $\tau_x = 60$ ps at $\Delta_\lambda = 0$ (Fig. 4a, b). The reduction in lifetime by a factor of 145 confirms that our QD is coupled to the cavity mode and spatially located near the cavity centre. Such short

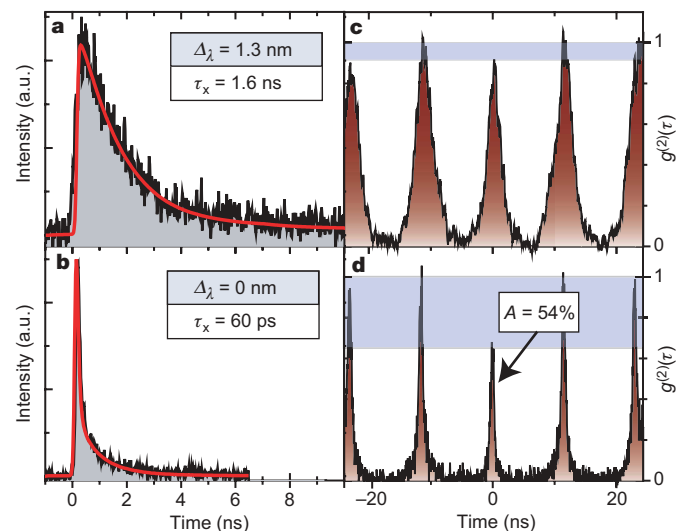


Figure 4 | Characteristics of the strong-coupling regime in the time domain. **a**, The exciton lifetime τ_x is reduced to 1.6 ns when the detuning is $\Delta_\lambda = 1.3$ nm. **b**, At exact spectral resonance, τ_x decreases to 60 ps, a reduction by a factor of 145 from the value at $\Delta_\lambda = 4.1$ nm. **c**, Autocorrelation function of the cavity mode off-resonance with the exciton, showing no significant quantum correlations. **d**, Autocorrelation of the strongly coupled cavity–QD system demonstrating strong quantum correlations in the form of photon antibunching, where the central peak area, A , is 54% of the area of peaks at other times. In **a** and **b**, histogram data are shown in black and an exponential fit in red. In **c** and **d**, the grey bar shows the difference between the central peak height and the average height at other times.

lifetimes, approaching the cavity photon storage time, support the spectral evidence that the exciton–photon coupling g is sufficiently large for the system to be in the strong-coupling regime. In order to estimate g independently from the Rabi splitting, we assume that τ_x is primarily determined by a lorentzian dependence on the detuning¹⁸, and fit the experimental data (see Methods) to obtain $g = 21.8$ GHz = 90 μeV , which agrees very well with the value obtained from the Rabi splitting.

The spectral anticrossing that we observe is unequivocally a result of strong coupling; however, we emphasize that the calculated two-peak lineshape also describes exactly two coupled classical harmonic oscillators¹⁹. Therefore, Rabi splitting alone is not sufficient to discriminate between a regime arising from the interaction of single exciton and photon quanta and a classical regime describing the coupling behaviour of two classical oscillators. For cavity photon occupation numbers above one, the quantum nonlinear regime is manifested in the Jaynes–Cummings ladder spectrum²⁰, which is absent in the case of two strongly coupled classical oscillators. A direct experimental demonstration of the quantum nonlinear regime has been reported for single atoms flying through microwave cavities²¹ and, in the case of optical cavities, has been inferred by monitoring the statistics of the emitted photon stream²². In QD cavity QED, in which the artificial atom is composed of many atoms embedded in a host matrix, it is crucial to confirm that the system manifests true quantum behaviour. To this end, we measure the second-order auto-correlation function $g_{m,m}^{(2)}(\tau)$ of the cavity photon stream under pulsed excitation. For $\Delta_\lambda = 4.1$ nm, the cavity displays nearly poissonian photon statistics as shown in Fig. 4c, with $g_{m,m}^{(2)}(0) \approx 1$, revealing its harmonicity. That is, the cavity is accepting multiple photons at the same time—a surprising result given the observed $g^{(2)}(0) \approx 0$ in cross-correlation with the exciton. We then tuned the system into strong coupling and measured the auto-correlation function of the entire three-peak structure consisting of the strong-coupling doublet and the pure photonic state of the cavity. In this regime, the statistics of the cavity photon stream dramatically change to sub-poissonian (Fig. 4d), with a central peak area at $\tau = 0$ that is only 54% of the average peak area at other times.

We note that the area of the peak at $\tau = 0$ is increased from the ideal value of zero by two mechanisms. First, the central peak in the observed spectral triplet, which is not antibunched, contributes 45% of the total collected photoluminescence, as determined by the three-lorentzian fit shown in Fig. 3b. Second, in strong coupling, the carrier capture process proceeds on timescales longer than the polariton decay time (13.3 ps), so that it is possible for the system to undergo multiple capture/emission events per excitation pulse. Accounting for these factors, the measured $g^{(2)}(\tau)$ shows clearly that the cavity field attains an anharmonic character when brought into strong coupling with the exciton, proving the interaction is with a two-level quantum system. We have confirmed that the main contribution to the peak at $\tau = 0$ is from the pure photonic state of the cavity by performing auto-correlation measurements on another device that exhibited larger Rabi splitting. In this device, we spectrally filtered a single polariton peak so that the pure photonic state of the cavity contributed only 15% of the total signal (Supplementary Fig. S1). In this case, the auto-correlation signal exhibited strong antibunching with a peak area at $\tau = 0$ of only 19% (Supplementary Fig. S2). These photon correlation measurements prove the quantum nature of the strongly coupled QD–cavity molecule.

A direct demonstration of the photon blockade effect²³ could be obtained by exciting the photonic channel of the strongly coupled system in reflection or transmission measurements, thereby reaching the ultimate limit of solid-state nonlinear optics at the single-photon level. The results of the present work encourage the experimental pursuit of quantum information tasks in the solid state, such as the deterministic coupling of two QDs mediated by a common cavity mode²⁴.

METHODS

Semiconductor material. The semiconductor heterostructure used for subsequent photonic crystal fabrication was grown on a (100) semi-insulating GaAs substrate by molecular beam epitaxy. The epitaxial structure consists of a 126 nm GaAs slab incorporating a layer of InAs quantum dots at the centre with a density ranging from zero to 3 per μm^2 across the sample. By annealing the quantum dots *in situ* when partially capped with GaAs, we tuned the quantum-dot ground state energies to ~ 1.3 eV. The photonic crystal slab is grown above a $1\ \mu\text{m}$ $\text{Al}_{0.7}\text{Ga}_{0.3}\text{As}$ layer that is later removed to provide vertical optical isolation.

Optical characterization. For micro-photoluminescence experiments, samples are mounted in a liquid-helium flow cryostat at 4.2 K. We excite with an above-bandgap ($\lambda = 780$ nm) continuous wave diode laser focused to a $1\ \mu\text{m}$ spot using a $50\times$ microscope objective (NA = 0.55). The photoluminescence signal is collected by the same objective, dispersed by a 750 mm grating spectrograph with a spectral resolution of 21 pm, and detected with a liquid-nitrogen-cooled charge coupled device camera.

In time-dependent lifetime measurements, we excite the sample with a Q-switched pulsed diode laser at a rate of either 40 MHz or 80 MHz. We spectrally filter the photoluminescence using the spectrometer (bandwidth = $0.4\ \text{nm} = 550\ \mu\text{eV}$) and focus it on an avalanche photodiode (APD) single-photon counter. A time-to-amplitude converter (TAC) transforms time differences between photon detection events and synchronization pulses provided by the laser to electrical signals of corresponding amplitude. A multichannel analyser accumulates a histogram of the measured intervals. We can choose between two different types of APDs to obtain time resolution of either ~ 70 ps or ~ 400 ps, with the latter having significantly higher quantum efficiency.

In auto-correlation measurements, filtered light is sent to a Hanbury Brown–Twiss interferometer, consisting of a 50:50 plate beam splitter with an APD at either output. Time-correlation of the signals is done in a manner similar to that in lifetime measurements. Cross-correlation measurements are done in the same way after the two wavelengths of interest are spatially separated by the spectrometer.

Estimation of g . We assume that τ_x is primarily determined by a Lorentzian dependence on the detuning¹⁸ and fit the experimental data with the relation $\hbar/\tau_x = \gamma_b + \gamma_{\text{SE}}$, in which γ_b is the background emission rate into all other modes and $\gamma_{\text{SE}} = \gamma_m g^2 / [A_\omega^2 + (\gamma_m/2)^2]$ is the spontaneous emission rate into the cavity mode. The best fit is given by $\gamma_b = 12.2\ \text{MHz} = 0.05\ \mu\text{eV}$ and $g = 21.8\ \text{GHz} = 90\ \mu\text{eV}$. The first value corresponds to a lifetime of 13 ns, strongly modified from the bulk lifetime by the photonic bandgap. The second value confirms that in our system the strong-coupling condition $g^2 > (\gamma_x - \gamma_m)^2/16$ is satisfied and agrees very well with the value of g estimated from the vacuum-field Rabi splitting.

Received 4 October 2006; accepted 8 January 2007.

Published online 28 January 2007.

- Mabuchi, H. & Doherty, A. C. Cavity quantum electrodynamics: Coherence in context. *Science* **298**, 1372–1377 (2002).
- Raimond, J. M., Brune, M. & Haroche, S. Colloquium: Manipulating quantum entanglement with atoms and photons in a cavity. *Rev. Mod. Phys.* **73**, 565–582 (2001).

- Painter, O. *et al.* Two-dimensional photonic band-gap defect mode laser. *Science* **284**, 1819–1821 (1999).
- Strauf, S. *et al.* Self-tuned quantum dot gain in photonic crystal lasers. *Phys. Rev. Lett.* **96**, 127404 (2006).
- Akahane, Y., Asano, T., Song, B. S. & Noda, S. High-Q photonic nanocavity in a two-dimensional photonic crystal. *Nature* **425**, 944–947 (2003).
- Wallraff, A. *et al.* Strong coupling of a single photon to a superconducting qubit using circuit quantum electrodynamics. *Nature* **431**, 162–167 (2004).
- Peter, E. *et al.* Exciton-photon strong-coupling regime for a single quantum dot embedded in a microcavity. *Phys. Rev. Lett.* **95**, 067401 (2005).
- Yoshie, T. *et al.* Vacuum Rabi splitting with a single quantum dot in a photonic crystal nanocavity. *Nature* **432**, 200–203 (2004).
- Reithmaier, J. P. *et al.* Strong coupling in a single quantum dot-semiconductor microcavity system. *Nature* **432**, 197–200 (2004).
- Badolato, A. *et al.* Deterministic coupling of single quantum dots to single nanocavity modes. *Science* **308**, 1158–1161 (2005).
- Hennessy, K., Badolato, A., Petroff, P. M. & Hu, E. L. Positioning photonic crystal cavities to single InAs quantum dots. *Photonics Nanostruct. Fund. Appl.* **2**, 65–72 (2004).
- Strauf, S. *et al.* Frequency control of photonic crystal membrane resonators by monolayer deposition. *Appl. Phys. Lett.* **88**, 043116 (2006).
- Kiraz, A. *et al.* Photon correlation spectroscopy of a single quantum dot. *Phys. Rev. B* **65**, 161303 (2002).
- Childs, J. J., An, K., Otteson, M. S., Dasari, R. R. & Feld, M. S. Normal mode line shapes for atoms in standing-wave optical resonators. *Phys. Rev. Lett.* **77**, 2901–2904 (1996).
- Yablonovitch, E. Inhibited spontaneous emission in solid-state physics and electronics. *Phys. Rev. Lett.* **58**, 2059–2062 (1987).
- Purcell, E. M. Spontaneous emission probabilities at radio frequencies. *Phys. Rev.* **69**, 681 (1946).
- Englund, D. *et al.* Controlling the spontaneous emission rate of single quantum dots in a two-dimensional photonic crystal. *Phys. Rev. Lett.* **95**, 013904 (2005).
- Andreani, L. C., Panzarini, G. & Gerard, J. M. Strong-coupling regime for quantum boxes in pillar microcavities: Theory. *Phys. Rev. B* **60**, 13276–13279 (1999).
- Pau, S., Bjork, G., Jacobson, J., Cao, H. & Yamamoto, Y. Microcavity exciton-polariton splitting in the linear regime. *Phys. Rev. B* **51**, 14437–14447 (1995).
- Haroche, S. *Fundamental Systems in Quantum Optics* (Elsevier, New York, 1992).
- Brune, M. *et al.* Quantum Rabi oscillation: A direct test of field quantization in a cavity. *Phys. Rev. Lett.* **76**, 1800–1803 (1996).
- Birnbaum, K. M. *et al.* Photon blockade in an optical cavity with one trapped atom. *Nature* **436**, 87–90 (2005).
- Imamoglu, A., Schmidt, H., Woods, G. & Deutsch, M. Strongly interacting photons in a nonlinear cavity. *Phys. Rev. Lett.* **79**, 1467–1470 (1997).
- Imamoglu, A. *et al.* Quantum information processing using quantum dot spins and cavity QED. *Phys. Rev. Lett.* **83**, 4204–4207 (1999).

Supplementary Information is linked to the online version of the paper at www.nature.com/nature.

Acknowledgements We acknowledge support by the Swiss National Research Foundation through the 'Quantum Photonics NCCR'.

Author Information Reprints and permissions information is available at www.nature.com/reprints. The authors declare no competing financial interests. Correspondence and requests for materials should be addressed to A.I. (imamoglu@phys.ethz.ch).